InSAR observations of ice elevation and velocity fluctuations at the Flade Isblink ice cap, eastern North Greenland

InSAR observations of ice elevation and velocity fluctuations at the Flade Isblink ice cap, eastern North Greenland

Steven J. Palmer,[1] Andrew Shepherd,[1] Aud Sundal,[1] Eero Rinne,[2] and Peter Nienow[2]

Received 15 April 2010; revised 6 October 2010; accepted 25 October 2010; published 21 December 2010.

[1] The 8500 km^2 Flade Isblink ice cap (FIIC) (81°15′N, 15°0′W) is the largest ice cap in Greenland. We use repeat-pass interferometric synthetic aperture radar (InSAR) techniques to investigate the form and flow of the FIIC. European Remote Sensing satellite (ERS-1 and ERS-2) data acquired in winter 1996 were used to form a 100 m resolution digital elevation model (DEM), which we constrained using Ice Cloud and Elevation satellite (ICESat) laser altimeter elevation measurements from 2007. This InSAR DEM was used to isolate the phase due to motion from seven ERS-tandem (1 day) pairs of SAR scenes acquired between 15 August 1995 and 7 February 1996, to produce one wintertime and two summertime velocity maps. Five of the eight major outlet glaciers draining the FIIC are marine terminating, and two terminate at a lake margin. A maximum ice velocity of 581 m yr^{-1} was observed in mid-August 1995. Six of the eight major outlet glaciers exhibit seasonal velocity variations between late summer and winter, and flow speeds vary by up to 20% over a 10 day period in August 1995. Our findings show that while marine terminating glaciers flow faster than land terminating glaciers, there is no simple relationship between glacier type and seasonality of ice motion.

Citation: Palmer, S. J., A. Shepherd, A. Sundal, E. Rinne, and P. Nienow (2010), InSAR observations of ice elevation and velocity fluctuations at the Flade Isblink ice cap, eastern North Greenland, *J. Geophys. Res.*, *115*, F04037, doi:10.1029/2010JF001686.

1. Introduction

[2] The Flade Isblink ice cap (FIIC) is situated in Kronprins Christian Land, eastern North Greenland (Figure 1) on Princess Dagmar Peninsula. With an area of 8500 km^2, it is the largest independent ice cap in Greenland [*Kelly and Lowell*, 2009]. The northern portion of the ice cap exhibits low surface slopes and reaches a maximum elevation of around 710 m. In contrast, the southern part overlays the Princess Elisabeth Alps and many nunataks are present. Surface gradients are generally steeper in the southern part of the ice cap and the maximum elevation is around 960 m. The earliest study of the FIIC [*Mikkelsen*, 1913] was restricted to ground-based observations of the basic geometry and extent of the ice cap. The FIIC was originally discovered in 1907 during the "Danmark" expedition led by Mylius-Erichsen, although it was not until the first aircraft surveys of this area in 1932 that the ice cap was discovered to be independent of the Greenland ice sheet [*Koch*, 1935]. The ice cap was observed to slope evenly and crevasse-free toward the Arctic Ocean in most places except at Antarctic Bay, where the ice terminated in steep walls, behind which existed extensive crevasse systems. *Helk and Dunbar* [1953] observed that FIIC was apparently inactive with a stagnant east side and a northern margin "disintegrating into flat-topped bergs."

[3] More recently, remote sensing studies have provided sparse observations of ice velocity and surface elevation changes. *Higgins* [1991] used aerial photographs acquired in 1961 and 1978 to track features of the FIIC in order to estimate the mean velocity at two locations shown in Figure 1. A 25 km broad outlet to the east of Station Nord was identified, extending northward as a floating glacier tongue up to 20 km long, although no significant iceberg calving events were reported during the survey period [*Higgins*, 1991]. Observed velocities were 360 m yr^{-1} at the western lobe (Figure 1, location 1) and 175 m yr^{-1} at the eastern lobe (Figure 1, location 2). *Krabill et al.* [2000] used aircraft laser altimeter observations from 1994 and 1999 to measure surface elevation changes at the FIIC. Mean thickening rates of 60 cm yr^{-1} were observed in the south and 40 cm yr^{-1} in the north, and up to 20 cm yr^{-1} of thinning occurred at the eastern margin. More recent ICESat observations showed a distinct longitudinal gradient in surface elevation change, with the western half of the FIIC having thickened by around 50 cm yr^{-1}, and the eastern half having thinned by around 20 cm yr^{-1} between 2003 and 2007 [*Pritchard et al.*, 2009]. A radio echo sounding survey of the FIIC carried out by the U.S. Center for Remote Sensing of Ice Sheets and the Danish Niels Bohr Institute during May 2006 showed that ice near to the ice cap summit is around 535 m thick (C. Laing, unpublished data, 2009), though was too wet for internal layers to be resolved.

[1]School of Earth and Environment, University of Leeds, Leeds, UK.
[2]School of GeoSciences, University of Edinburgh, Edinburgh, UK.

0148-0227/10/2010JF001686

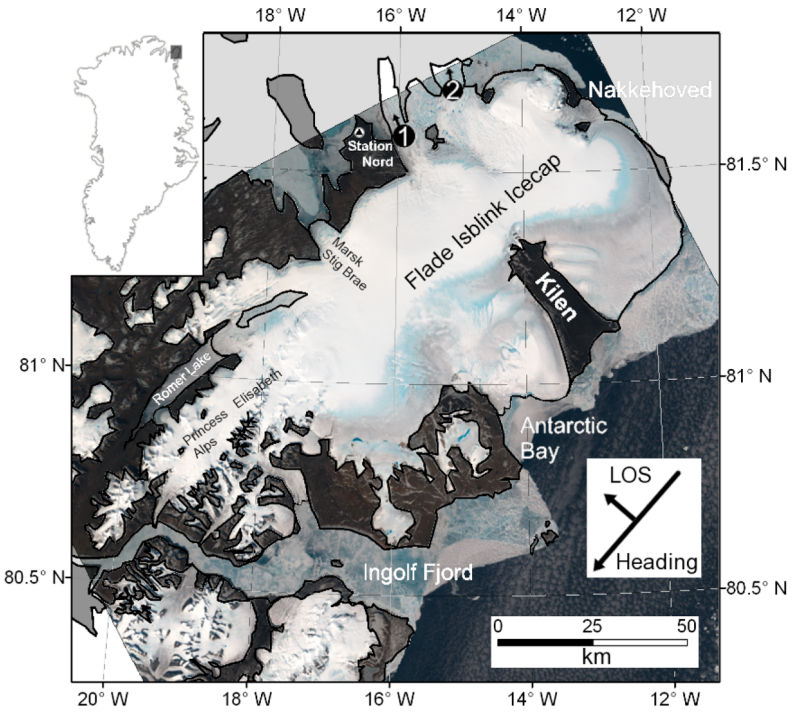

Figure 1. Location map of the Flade Isblink ice cap (FIIC), with satellite heading and radar line-of-sight (LOS) indicated. The locations (numbers 1 and 2) of previous velocity estimates [*Higgins*, 1991] discussed in the text are also shown. The background is a Landsat image acquired on 3 July 2001.

In addition, *Hall et al.* [2008] have compared satellite-based Moderate Resolution Imaging Spectroradiometer (MODIS) measurements of surface temperature to in situ observations and found that there was no variation in surface temperature with elevation on 3 July 2001 and on 23 June 2004, suggesting that the entire ice surface of the FIIC was at or near to melting on these dates. Here we use InSAR techniques to form a new 100 m resolution elevation model and the first velocity maps of the FIIC, in order to investigate flow variations of the main outlet glaciers between summer 1995 and winter 1996.

2. Data

[4] We use 14 ERS SAR images acquired between 20 July 1995 and 7 February 1996 (Table 1) to calculate the surface elevation and velocity of the FIIC. During this tandem-mission period, the ERS-2 satellite followed the ERS-1 satellite in a near-identical orbit, 1 day behind. The short time interval between acquisitions ensures that interferometric coherence is maintained as the surface changes little during the intervening period. SAR data acquired during the ERS tandem mission have proved to be a key data set for studies of the cryosphere and have been used to map velocity over large areas [e.g., *Shepherd et al.*, 2001], grounding line retreat [e.g., *Rignot*, 1998] and melting at the base of floating ice [e.g., *Joughin and Padman*, 2003]. We obtained raw SAR scenes and processed them to single-look complex (SLC), slant-range image data with a ground resolution of ~50 m in both range and azimuth for our interferometric analysis [*Werner et al.*, 2000]. These image frames typically cover 100 km by 100 km. The data were recorded during descending satellite orbits, when the satellite ground track was almost parallel to the long axis of the FIIC (see Figure 1), resulting in a favorably oriented radar look direction for 7 of the 8 outlet glaciers observed. From these data, we assembled 7 pairs of SAR images separated by 1 day that were suitable for interferometry.

[5] We use point measurements of elevation acquired by the Geoscience Laser Altimeter System (GLAS) instrument onboard NASA's Ice Climate and Elevation satellite (ICESat) [*Zwally et al.*, 2003] to constrain and validate our interferometric data set. The GLAS provides measurements of elevation along the satellite ground track of 65 m spatial resolution at 172 m spacing [*Zwally et al.*, 2002b; *Schutz et al.*, 2005]. The ICESat reference orbit follows a 91 day exact repeat, with a 33 day subcycle [*Schutz et al.*, 2005]. We use GLAS Level 1B elevation data (GLA06) recorded in 2007, which includes corrections for atmospheric propagation delays and the effect of solid Earth tides [*Brenner et al.*, 2003], to provide an improved estimate of the interferometric baselines and to validate an elevation model that we produce from InSAR. We also use an existing, coarse resolution DEM of the Greenland Ice Sheet (GrIS), gridded at 1 km horizontal spacing [*DiMarzio et al.*, 2007] as part of the validation exercise. This DEM was produced from data acquired during the first seven operational periods (from February 2003 through June 2005) of the GLAS instrument.

[6] Finally, we use local air temperature measurements to aid our interpretation of the FIIC velocity data set. Daily maximum air temperature measurements were acquired at Station Nord (81°36′N, 16°41′W) automatic weather station

Table 1. SAR Data Used in This Study

Date	Day Number	Sensor	Orbit	Frames	$B_\perp$ (m)	Use
15 Aug 1995	227	ERS1	21355	1939	−2	day 228 InSAR velocity
16 Aug 1995	228	ERS2	1682	1939	−2	day 228 InSAR velocity
24 Aug 1995	236	ERS1	21484	1920,1931	1	day 237 InSAR velocity
25 Aug 1995	237	ERS2	1811	1920,1931	1	day 237 InSAR velocity
2 Jan 1996	367	ERS1	23359	1929,1939	8	InSAR DEM winter InSAR velocity
3 Jan 1996	368	ERS2	3686	1929,1939	8	InSAR DEM winter InSAR velocity
6 Feb 1996	402	ERS1	23860	1929,1939	200	InSAR DEM winter InSAR velocity
7 Feb 1996	403	ERS2	4187	1929,1939	200	InSAR DEM winter InSAR velocity

(AWS) between January 1986 and May 2009 (www.tutiempo.net). The data set provides a near-continuous record of air temperature in the vicinity of the FIIC, although no data were available for the periods September 1988 to January 1989, September to November 1999, September 2003 to September 2005, November 2005 and March to July 2007.

3. Methods

[7] We processed 14 ERS tandem SAR scenes to determine the surface elevation and velocity of 90% of the FIIC. From these data, we formed 2 winter and 2 August interferograms, which were sensitive to both surface movement in the radar line-of-sight (LOS) during the acquisition period and to the topography of the ice cap surface [*Joughin et al.*, 1998]. Differential InSAR was used to produce a topography-only interferogram [*Kwok and Fahnestock*, 1996] which was then converted to absolute heights [*Joughin et al.*, 1998] using ICESat elevation measurements [*Zwally et al.*, 2003]. This InSAR DEM was used to remove topographic phase from the remaining interferograms in order to isolate the velocity signal [*Kwok and Fahnestock*, 1996]. The methods for each step are described in detail below.

3.1. Raw Data Processing

[8] The raw ERS data were processed to SLC format using a commercially available SAR processor [*Werner et al.*, 2000] and precise orbit data [*Scharroo and Visser*, 1998]. Corrections were made to compensate for the antenna gain patterns, nonzero doppler centroids and variations in doppler frequency along-track caused by squint [*Werner et al.*, 2000]. We extended the near and far range in each SAR data set to form images 2808 range pixels wide. Range compression, azimuth auto-focusing and azimuth compression were then applied. The SAR images were multilooked to reduce speckle noise by 2 in the range direction and 10 in the azimuth direction [*Werner et al.*, 2000]. Each SAR image pair was coregistered to within a few pixels using precision satellite state-vector data [*Gens and van Genderen*, 1996], followed by fine coregistration to a fraction of a pixel by comparing roughly corresponding areas and solving for a set of local transformation parameters [*Massonnet and Feigl*, 1998]. Complex interferograms containing both the amplitude and phase information were then formed by multiplying each complex pixel of the primary image by the complex conjugate of the corresponding pixel in the secondary image.

3.2. InSAR DEM

[9] We differenced the 2 winter interferograms to form a topography-only interferogram with an effective perpendicular baseline of 192 m. Although variations in winter velocity may occur [e.g., *Iken and Truffer*, 1997] insufficient data were available to demonstrate the scale of this variability and so we assumed a constant winter velocity. We calculated the altitude of ambiguity, which is a measure of the sensitivity to topography, to be 50 m. This differential interferogram was corrected for the effect of Earth's curvature and filtered with a window size of 32 then again with a window size of 8 to reduce phase noise. As the interferometric phase is measured in modulo 2π, phase unwrapping was applied to convert to continuous phase at each point as described by *Rosen et al.* [1994]. The unwrapped interferometric phase, together with the precision baseline estimate is then used to derive the topographic heights. Absolute surface elevation can only be retrieved with the use of tie points of known elevation [*Mohr*, 1997]. As InSAR-derived height maps contain relative values only, they require adjustment to yield absolute values. In the absence of contemporaneous elevation data, we achieved this by applying least squares fit of the unwrapped phase to ~500 point elevation measurements from ICESat in 2007. An improved estimate of the interferometric baseline was achieved in the same way [*Joughin et al.*, 1998]. Another high-Arctic study using ICESat data as ground control for an ERS-tandem InSAR-derived DEM estimated the resulting DEM error to be 6.3 m [*Atwood et al.*, 2007] and we expect our DEM to have a similar error. Although the InSAR and ICESat data used in this study were acquired ~10 years apart, the maximum expected changes in elevation of −2 m to +6 m during this period [*Krabill et al.*, 2000] are of similar magnitude to the expected DEM error and are assumed to have an insignificant impact within our calculated error limits. The data were then geocoded into UTM zone 28N to form a new DEM of the FIIC with a grid spacing of 100 m.

[10] Surface catchments were derived from the InSAR DEM using a hydrologic model [*Maidment*, 2002]. Local topographic minima were filled and flow direction for each cell was then calculated from the direction of steepest slope. Stream segments were defined and grouped into individual catchments, which were used to derive glacier boundaries. Due to uncertainties in the catchment delineation method, the smallest catchments were omitted from this analysis. Figure 2 shows the InSAR DEM and surface-derived surface catchments for the 8 major outlet glaciers.

3.3. InSAR Velocity

[11] We used the InSAR DEM to subtract topographic phase from other interferograms in order to isolate displacement in the radar LOS. As with the computation of topography, phase was unwrapped from modulo 2π to generate a continuous phase field. Calibration was achieved

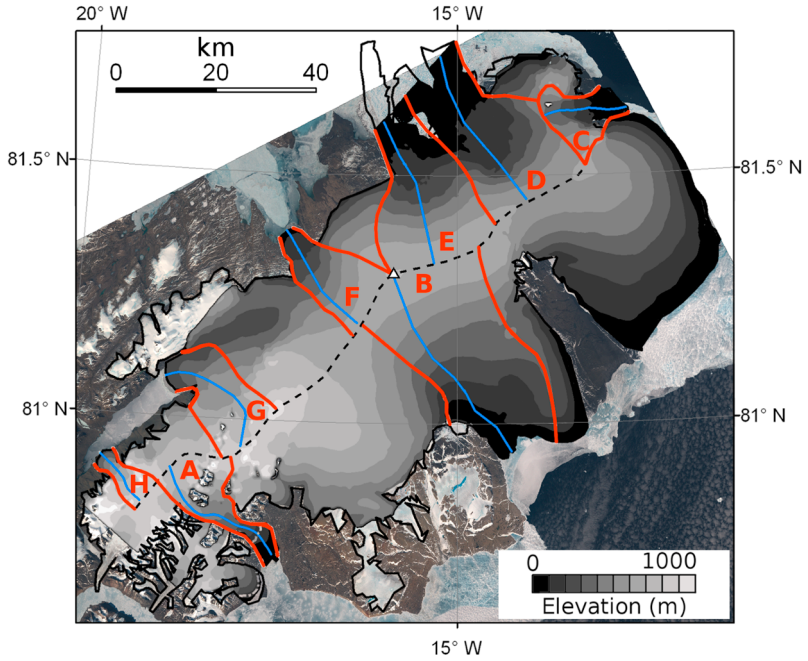

Figure 2. InSAR-derived DEM of the FIIC at 100 m intervals (greyscale) showing summit ridge (dashed black line), major surface catchments (thick red lines) and locations of outlet glacier transects (thin blue lines) shown in Figure 4. Also shown is the position of the central summit (white triangle) at an elevation of 710 m, where ice thickness has been measured to be 535 m (Laing, unpublished data, 2009).

by a least squares fit for phase values at the ice divide, which were assumed to have zero motion. Assuming surface-parallel flow in the direction of steepest slope, we were able to convert LOS displacements to ice velocity estimates over the FIIC for the dates of our interferograms [*Joughin et al.*, 1995]. To compute the ice flow direction, we averaged the elevation model over 2000 m, which is equal to approximately 10 times the mean ice thickness [*Paterson*, 1994]. In all cases, the phase coherence was sufficiently high to allow phase unwrapping all the way from the summit ice divide, to the glacier margin or edge of the scene. Therefore, in situ measurements of velocity were not necessary to constrain the velocity estimation. In this way we were able to estimate the average rate of ice motion over 24 h for day numbers 228, 237, 368 and 403 relative to 1 January 1995 (Table 1). The assumption of invariant winter flow made when forming the DEM is supported by the fact that the RMS value and standard deviation of the differences in the 2 resulting winter velocity maps are 8.5 m yr^{-1} and 6.3 m yr^{-1}, respectively. As the two winter interferograms (days 368 and 403) showed similar flow, we combined them to form a a mean winter velocity map for comparison with the August velocity maps. This mean winter map is weighted by the inverse of the interferometric baseline of the constituent velocity maps in order to minimize the effect of any topographic errors.

[12] The baselines associated with 6 of the 7 SAR image pairs used to estimate ice speed were below 10 m, resulting in interferograms which were insensitive to topographic errors [*Goldstein et al.*, 1993; *Joughin et al.*, 1996]. By calculating ice speed over 1200 km^2 of ice-free ground adjacent to the FIIC on day 237, we estimated the topographic error in our measurements of ice speed to be 7 m yr^{-1} (RMS value is 6.9 m yr^{-1}) on day 237. Similar analysis for the other days yields topographic error estimates of 3.2 m yr^{-1} for day 228, 3.0 m yr^{-1} for day 368 and 22.0 m yr^{-1} for day 403. In addition, we estimated the total LOS error from the calculated ice speeds along the main ice divide of the ice cap, where we would expect ice flow speeds to be zero. The RMS value of observed ice speeds at the main ice divide was 3.5 m yr^{-1} on day 237; 6.3 m yr^{-1} on day 228; 2.5 m yr^{-1} on day 368; and 5.7 m yr^{-1} for day 403. Even with reliable independent knowledge of the ice-flow direction, the accuracy of the resultant velocity estimate may be poor when this direction is close to orthogonal to the radar LOS direction, for which there is no sensitivity to displacement. The orientation of the radar LOS was oriented parallel to the direction of ice flow away from the central ice divide of the FIIC, thereby minimizing errors for these glaciers. The error in the velocity estimates at glacier C is likely to be larger due to the unfavorable radar LOS.

4. Results and Discussion

4.1. InSAR DEM

[13] The InSAR DEM was generated with a ground resolution of 100 m (Figure 2), and covers the majority (7700 km^2, equivalent to 91% of the ice area) of the FIIC. We compared it to ~40,000 point measurements of elevation determined by the ICESat satellite laser altimeter during the period 2003 to 2009 [*Zwally et al.*, 2003], excluding data from 2007 which was used to adjust the InSAR DEM. The RMS difference between the InSAR DEM and these ICESat point measurements of elevation was 12 m,

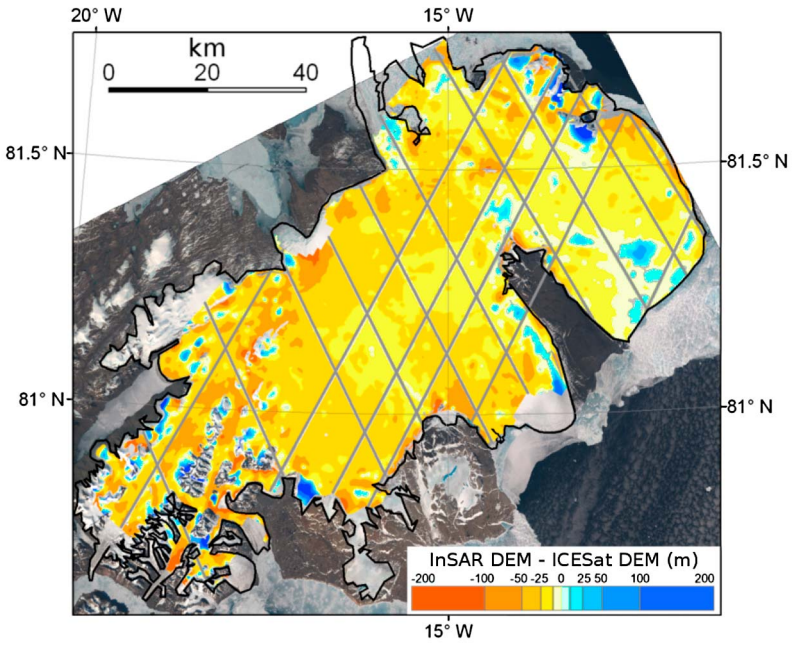

Figure 3. Differences in InSAR and ICESat DEMs (InSAR DEM minus ICESat DEM). Locations of ICESat point data flight lines used for adjusting the InSAR DEM are shown in gray. A SAR backscatter amplitude image is shown in the background, and the ice margin is shown as a thick black line.

compared with 10 m for the RMS difference between an existing DEM [*DiMarzio et al.*, 2007] and the same ICESat point measurements.

[14] We compared our InSAR DEM with a previous ICESat-derived DEM [*DiMarzio et al.*, 2007] of the ice cap (Figure 3). The RMS difference between the InSAR DEM and the ICESat DEM is 30 m (standard deviation is 43 m). The largest differences are in areas between ICESat ground tracks where elevation values have been interpolated in the ICESat DEM. The InSAR DEM reveals small-scale features located between ICESat ground tracks as well as the location of the ice margin. The maximum elevation of the FIIC is estimated to be 960 m. Ice thickness at the central summit has been measured to be 535 m (Laing, unpublished data, 2009). We estimate the surface elevation to be 710 m at the central summit and so the ice cap is grounded 175 m above sea level (m.a.s.l.) at this location.

[15] Differences between our InSAR DEM and the ICESat DEM are due to a combination of errors in the ICESat and InSAR data, measurement of different surfaces due to penetration of SAR signal and detection of real changes in the geometry of FIIC between 1996 and 2003–2005. It is important to highlight the fact that as ICESat data were used as ground control for the InSAR DEM, the two data sets are not independent and geographically correlated errors will not be detected. A previous comparison of the GLAS/ICESat laser altimetry Greenland DEM to a 5 km gridded radar altimetry DEM data set [*DiMarzio et al.*, 2004] indicated that the mean elevation difference of regions with surface slopes of 0.1° to 1.0° slopes is −24 ± 20 m, though this increases with local slope. At elevations above 600 m, our InSAR DEM consistently yields lower elevations than the ICESat GLAS (Figure 3). This is consistent with previous estimates of C band radar penetration of dry snow in the percolation zone of up to ~15 m [*Hoen and Zebker*, 2000; *Dall et al.*, 2001]. Previous observations made between 1994 and 2007 suggest an elevation change rate of up to 60 cm yr^{-1} [*Krabill et al.*, 2000; *Pritchard et al.*, 2009] suggesting that differences in elevation between the 1996 InSAR DEM and the 2003–2005 ICESat flightline data of up to 5 m can be attributed to changes in the geometry of the FIIC.

[16] We examined the InSAR DEM and Landsat data acquired on 3 July 2001 (Figure 2) to establish which glaciers of the FIIC were land terminating and which were marine terminating. The termini of glaciers A, B, C, D, E and F appear to meet the sea (Figure 2), and near-zero surface elevations at the termini of glaciers A, B, C and D (Figure 4) suggest they are floating at their termini. Our InSAR DEM covers all but the lowermost 10 km of glacier E and we observe the surface elevation to be 70 m at the edge of the DEM coverage. Although the glacier appears to meet the sea, the lack of complete coverage prevents us from determining the elevation at the terminus. While surface elevation at the terminus of glacier F is above the RMS error of our DEM, this alone is insufficient to determine whether the glacier is floating or grounded. Glaciers G and H terminate above sea level and flow into the Romer lake (Figures 2 and 4).

[17] Our InSAR DEM was used to delimit 8 glacier surface drainage basins, which range in area from 83 km^2 to 1048 km^2 (Table 2 and Figure 2). The largest of the surveyed catchments (glaciers B, D and E) flow orthogonal to the NE-SW oriented summit divide and are found in the central parts of the FIIC, while the smallest catchments (A, C and H) are located at the northern and southern limits of the ice cap. We extracted elevation profiles from the

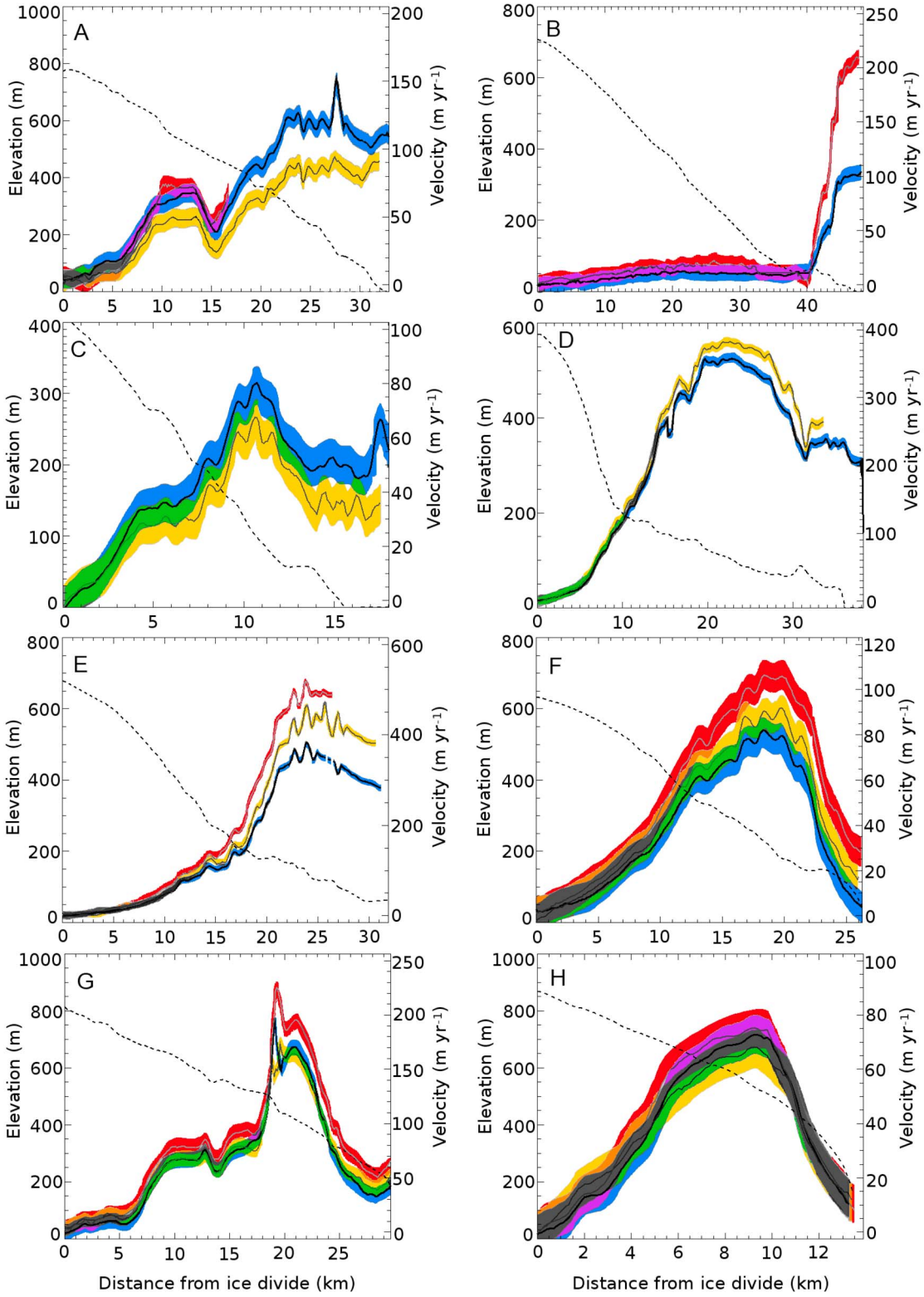

Figure 4. (a–h) Along-transect InSAR-derived elevation (dashed line), winter (days 368 and 403) velocity (blue), day 228 velocity (red) and day 237 velocity (yellow) for catchments A to H shown in Figure 2, with associated error bounds. Alternative colors are used where velocity estimates overlap (purple for winter/day 228, green for winter/day 237, orange for day 228/day 237, and gray where all three velocity estimates overlap).

Table 2. Outlet Glacier Statistics and Attributes[a]

Basin	Area (km^2)	Length (km)	Type[b]	Velocity, Winter 1996 (m/yr)		Velocity, Day 228 (m/yr)		Velocity, Day 237 (m/yr)		Position of Max Velocity	
				Mean	Max.	Mean	Max.	Mean	Max.	Distance From Ice Divide (km)	Elevation (m)
A	219	33	M	70	152	36*	75*	25	94	27.5	140
B	1048	48	M	19	118	38	222	21*	24*	48	0
C	203	19	M	43	73	-	-	30	63	10.5	100
D	751	42	M	212	357	-	-	224	377	22.5	100
E	636	32	-	156*	383*	178*	518*	162*	472*	24	150
F	299	26	MG	38	80	55	106	36	84	18.5	220
G	398	30	L	66	193	79	225	65	173	19	500
H	83	13.5	L	42	79	50	83	39	68	9.5	550

[a]Asterisks denote values from data sets with partial coverage of the glacier catchment.
[b]Abbreviations refer to whether the glacier is marine terminating and floating (M), marine terminating and grounded (MG), or lake terminating (L).

InSAR DEM along the centerlines of each of the surveyed outlet glaciers (Figure 4) of the FIIC in order to investigate the geometry of each glacier. While surface slopes at glaciers A, B and C are almost constant along their entire length, glacier D exhibits a distinct break in slope 9 km from the ice divide (Figure 4d). Above this break in slope, the topography of glacier D follows a convex profile from the ice divide at 600 m.a.s.l. down to the slope break at 200 m.a.s.l. and the average slope of this section of the glacier is 2.5 degrees. Below the break in slope, the topography of glacier D follows a different profile; there is an abrupt change to an undulating surface of low slope (Figure 4d) at a distance of 37 km from the ice divide. There are also several local topographic maxima along this section of the profile, most notably at 31 km from the ice divide. The surface elevation of transect E (Figure 4e) shows a similar bimodal profile to transect D; a break in slope after 14 km at 270 m.a.s.l. elevation separates the smooth and steep terrain exhibiting a convex profile at higher elevations from undulating low-gradient terrain at lower elevations. Glacier H (Figure 4h) exhibits the steepest mean slope of 3 degrees; elevation decreases from around 860 m.a.s.l. down to 150 m.a.s.l. at the glacier terminus 13.5 km from the ice divide.

4.2. Velocity Data

[18] Along each of the glacier center flow lines shown in Figure 2, we extracted InSAR velocity estimates (Figure 4 and Table 2). We investigated the extent to which the land terminating and marine terminating glaciers surveyed exhibited differing velocity profiles. Peak velocity at tidewater glaciers occurred at a mean elevation of 100 m, compared with 400 m for land terminating glaciers (Table 2 and Figure 4). At glacier B, peak velocity occurs at the glacier terminus while at glacier D it occurs roughly halfway down the glacier. Peak velocity at the remaining glaciers occurred at an intermediate position and was on average at a location 0.7 of the glacier length from the ice divide. Velocities at the terminus were on average about 200 m yr^{-1} for marine terminating glaciers in contrast to 30 m yr^{-1} for land terminating glaciers.

[19] Winter InSAR velocity (days 368 and 403) estimated at the FIIC is shown in Figure 5a. The winter velocity data set covers 90% of the FIIC; the mid-August (day 228) velocity data set covers 60% of the FIIC and the late August (day 237) velocity data set covers 82% of the FIIC. A maximum winter velocity of the FIIC of 434 ± 7 m yr^{-1} was observed at glacier E, which increased to 581 ± 7 m yr^{-1} at the same location on day 228. Flow averaged over the length of the central flow line is highest for the adjacent glacier D (212 m yr^{-1}), and shows seasonal variations of around 5%. Slowest flow occurs during winter at glaciers C and H, while the lowest flow line-averaged speed is at catchment B (19 m yr^{-1}). Low-velocity values at the terminus of glacier F, combined with the nonzero surface elevation at the terminus suggest the glacier is grounded. Velocity measured along the centerline of glacier G has an unusual profile shape as shown in Figure 4g. The winter InSAR velocity peaks sharply to 200 ± 7 m yr^{-1} at 19 km, after which it decreases to 150 ± 7 m yr^{-1} at 20 km and after which there is a second broader peak in ice speed of 170 ± 7 m yr^{-1} at 21 km. Below this there is a decrease to 30 ± 7 m yr^{-1}, 2 km from the ice margin, then an increase to 40 ± 7 m yr^{-1} at the ice front. The sharp peak in velocity at 19 km corresponds to a section of steep slope as shown in the elevation profile (Figure 4g).

4.3. Ice Speed Temporal Change

[20] Ice flow speeds at the majority of the surveyed area of the FIIC are similar or greater in late summer than in winter. For example, ice flow speeds on days 228 and 237 (Figures 4b and 4c) exceeded wintertime (days 368 and 403) rates by 10 m yr^{-1} or more for 39% and 30% of the surveyed ice cap area, respectively. In contrast, 0.5% and 2% of the surveyed area was observed to be flowing at speeds of more than 10 m yr^{-1} below the wintertime rates. Within catchments A and C, we observe slower ice speeds in late summer than in winter (Figures 4a and 4c). Although temporal fluctuations in velocity are observed at all glaciers, those recorded at glacier H are of comparable magnitude to the estimated measurement error of ±10 m yr^{-1}. The surveyed outlet glaciers of the FIIC exhibit a range of temporal fluctuations in ice flow speed which we broadly group into (1) glaciers exhibiting seasonal variations in ice flow speeds and (2) glaciers showing no significant seasonal variation in flow speeds. We discuss these findings in more detail below.

[21] Glacier A exhibits significant temporal variations in ice flow speeds (Figure 6). Velocity observed on day 237 follows a similar profile to winter, though 30 ± 10 m yr^{-1} slower, peaking at 95 ± 7 m yr^{-1} at 27.5 km. Day 228 data

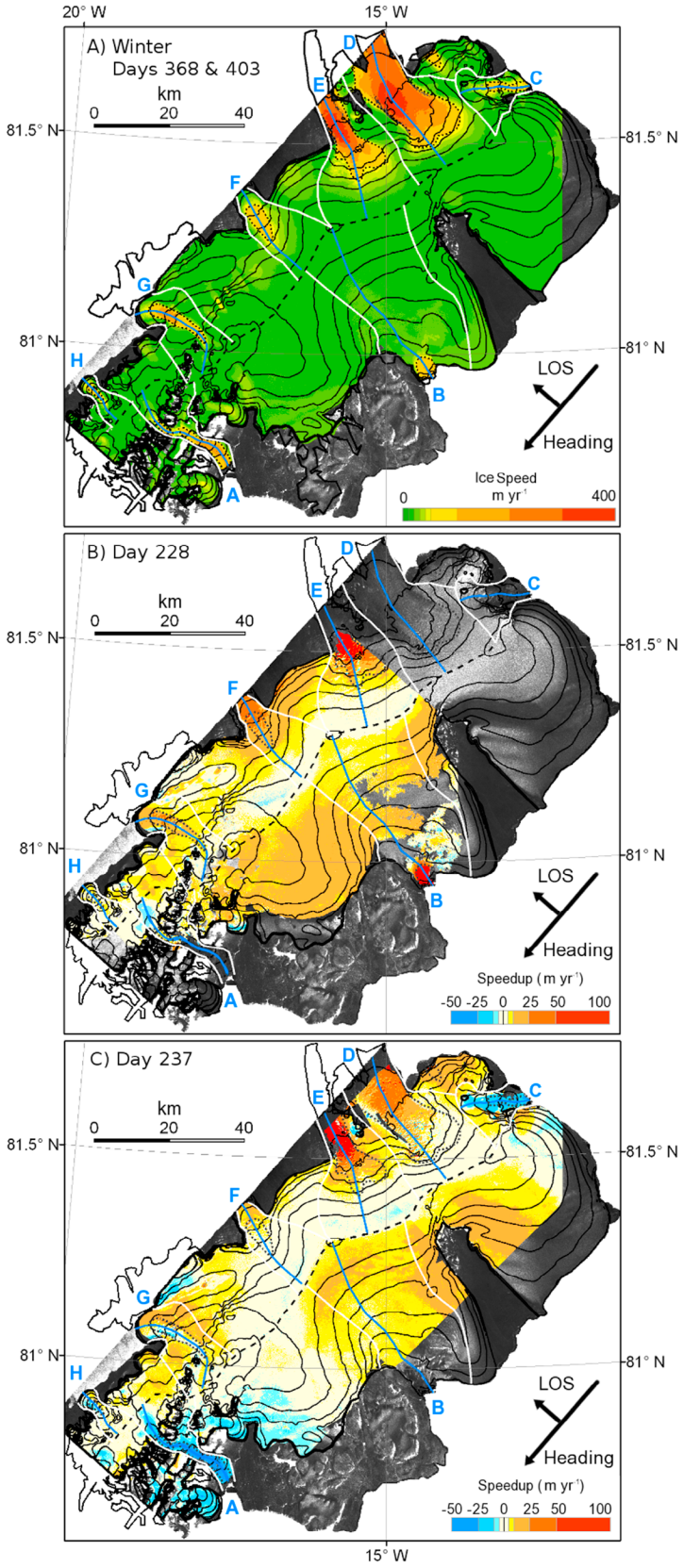

Figure 5. (a) Winter velocity measured during winter 1996. Elevation contours at 100 m intervals and ice cap margin are shown in black. Shown inset are the directions of satellite heading radar and line-of-sight (LOS). The background is a SAR backscatter amplitude image. Speedup above winter speeds (2 January 1996 and 6 February 1996) on (b) day 228 (15 August 1995) and (c) day 237 (24 September 1995).

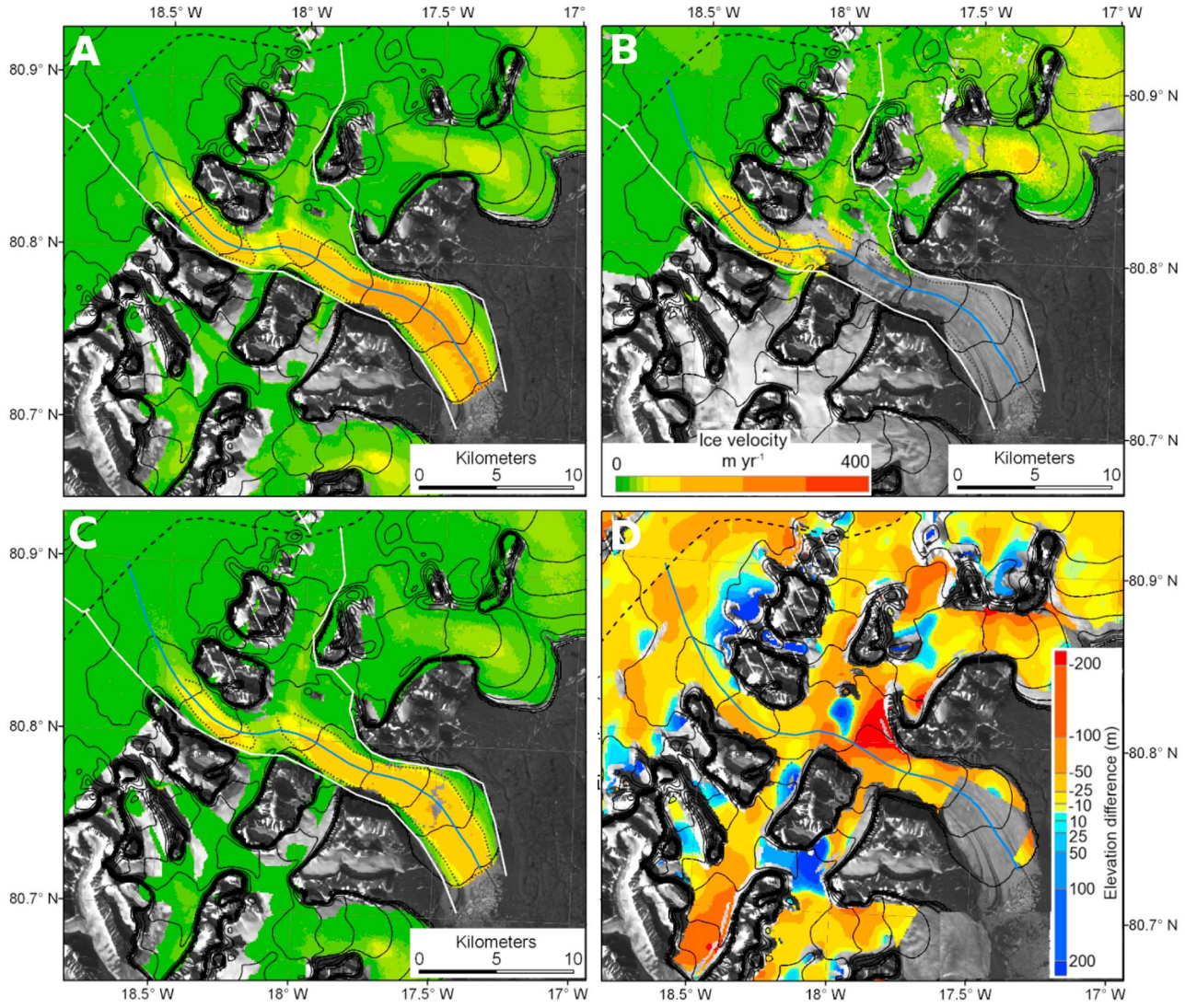

Figure 6. Enlargement of catchment A (see Figure 2) showing velocity estimated from InSAR (a) during winter 1996 (2 January 1996 and 6 February 1996), (b) on day 228 (15 August 1995), and (c) on day 237 (24 August 1995). Also shown is (d) the elevation difference between the InSAR and ICESat DEMs [*DiMarzio et al.*, 2007] shown in Figure 3.

was unavailable below 16.5 km from the ice divide. Glaciers B, C, D, E and F also exhibit significant seasonal changes in ice flow speed. At glacier E, speeds observed on both the day 228 and day 237 are higher and exhibit similar along-glacier profiles to winter. Seasonal differences in ice speed are within error for most of Glacier C, though near the terminus, winter speed is double that of day 237 speed. Although day 228 data does not extend over the whole of glacier D and day 237 data does not extend over the whole of glacier B, we include both glaciers in this group. At glacier B, day 228 velocity increases to roughly double the winter rate near the terminus. Ice speed measured at glacier D on day 237 exhibits a similar profile shape to winter and is around 30 ± 10 m yr^{-1} faster than winter speed over the final few kilometers. At glacier F, both day 228 and day 237 velocity follow a similar profile to winter velocity. Velocity differences above the winter at the terminus are 25 ± 10 m yr^{-1} on day 228 and 12 ± 10 m yr^{-1} on day 237.

[22] Glaciers G and H exhibit seasonal changes in speed within the error of ±10 m yr^{-1} and we classify them as having no significant seasonal changes in ice flow speed. However, ice flow at glacier G on day 228 ice speed is up to 20% higher than on day 237. Glacier H shows little variation from winter velocities during late summer, and the maximum velocity difference between mid-August and late August is a decrease of 10 ± 10 m yr^{-1}. Ice within the final few kilometers shows a higher variability in ice speed in late August than in winter.

[23] We examined the extent to which there is agreement between the speed estimates derived from InSAR and previous observations from aerial photos. We observe faster flow at glacier D than was observed by a previous study [*Higgins*, 1991] suggesting that the glacier was flowing at around 45 m yr^{-1} (~20%) faster in 1996 than it was during the period 1961 to 1978. However, it is important to highlight the large differences in the duration and timing of the

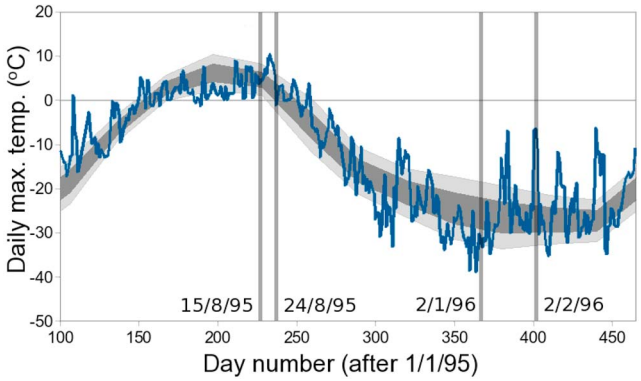

Figure 7. Daily maximum temperature at Station Nord (elevation 36 m.a.s.l.) (blue), plotted over the monthly mean of daily maximum temperatures for the period January 1986 to June 2009 ±1 standard deviation (dark gray) and ±2 standard deviations (light gray). Vertical bars show the acquisition dates of the SAR data used to produce the InSAR velocity maps.

observations, which means that any cyclical changes in ice flow speeds may have been aliased, making comparisons of the observations less meaningful. According to a recent study of ICESat elevation data, the lower reaches of catchment D have thinned by around 40 cm between 2003 and 2007 [*Pritchard et al.*, 2009]. This thinning is anomalous when compared to changes observed at the remainder of the western half of the FIIC, which thickened by around 2 m over the same period [*Pritchard et al.*, 2009].

[24] Together with the results of a previous study [*Higgins*, 1991], our data provide evidence for both seasonal and interannual fluctuations in the rate of ice flow at the FIIC. The lower portion of glaciers A and C showed higher velocities in winter than late August (with no data in mid-August), and the upper portion of glacier A showed higher winter velocities than mid- or late August. Glaciers B, D and E showed slowest flow in winter, fastest flow in mid-August and intermediate velocities in late August. We show that glacier E exhibited small (5%) variation in velocity between winter and August. Glacier F sped up in mid-August but returned to winter velocity at the end of August. Although no significant seasonal velocity differences were observed at glaciers G and H, it is possible that they experienced a seasonal speedup earlier in the summer and returned to winter speeds before late August.

[25] Other authors [e.g., *Iken*, 1974; *Bingham et al.*, 2003; *Boon and Sharp*, 2003] have observed changes in the rate of ice motion at Arctic glaciers and these have been attributed to seasonal variations in the amount of meltwater available for basal sliding. Similar observations have been made at the western margin of the GrIS [*Zwally et al.*, 2002a; *Das et al.*, 2008; *Shepherd et al.*, 2009; *Bartholomew et al.*, 2010]. Figure 7 shows that at the time of the fastest observed flow (day 228, 16 August 1995), the daily maximum air temperature measured at Station Nord (elevation 36 m.a.s.l.) was 4.5°C (mean daily temperature was 4.2°C), which is typical for this time of year. Using an August atmospheric lapse rate of 0.5°C 100 m^{-1} [*Steffen and Box*, 2001], the melting level was at 900 m.a.s.l., meaning that almost the entire ice cap was above freezing and runoff may have been available to enhance sliding across all catchments. Slower-than-winter ice speeds observed on day 237 at glacier A could be explained by the unusual meteorological conditions around the time of the August observations. Figure 7 shows that between day 228 and day 237, daily maximum temperatures measured at Station Nord were unseasonably high; up to 10.4°C with 5 of the 9 intervening days having a daily mean air temperature above 5°C. However, temperature measured on day 237 had a mean value of −1.2°C and a maximum of −1°C at Station Nord, representing an unseasonal "cold snap." It is possible that the slower-than-winter velocities we observe during late summer at glaciers A and C and the differences in ice speed observed on days 228 and 237 at glacier G are a transient dynamic response to changes in the amount of surface melting.

5. Conclusions

[26] We have used InSAR techniques to produce a fine-resolution digital elevation model of the Flade Isblink ice cap in eastern North Greenland, and also to produce the first ice velocity maps of the ice cap. Each of the two summertime and two wintertime velocity maps represent 24 h of motion and were acquired between 15 August 1995 and 3 February 1996.

[27] Our 100 m resolution InSAR DEM covers 91% the FIIC surface area and is of comparable accuracy to a widely used DEM of this area [*DiMarzio et al.*, 2007]. It reveals ice surface geometry in detail and provides information on the characteristics of the 8 major outlet glaciers, which we have categorized into 3 groups; those which are marine terminating and appear to be floating at their termini (A, B C and D), those which are marine terminating but grounded (F), and those which flow into a lake above sea level (G and H). While glacier E appear to be marine terminating, lack of complete DEM coverage prevents us determining if it is floating at the terminus. The DEM was used to delineate ice surface drainage basins, which range in area from 83 km^2 to more than 1000 km^2. Tidewater glacier catchments have on average twice the area of land terminating catchments. There are differences (RMS difference is 30 m) between our DEM and a previous DEM [*DiMarzio et al.*, 2007], which we suppose arise due to a combination of radar penetration in the percolation zone, detection of surface elevation changes (for the period 1996 to 2003–2005) and inherent errors in each of the elevation models.

[28] We mapped velocities of 90% of FIIC in winter 1996, 82% in mid-August 1995 and 60% in late August 1995. Summer velocities were observed to be higher than winter velocities for around one third of the FIIC and are observed to be more variable than winter velocities. Two of the marine terminating glaciers exhibit slower-than-winter flow during late August, which we suggest may be due to a transient dynamic response to changes in surface melting. We observe 20% faster ice flow in winter 1996 than the mean flow observed between 1961 and 1978 in a previous study [*Higgins*, 1991], although the observation periods varied in duration. A greater variation in the position of peak velocity is observed for marine terminating glaciers than for land terminating glaciers. Peak velocity occurred roughly 0.7 of the distance between the ice divide and terminus for

two thirds of the glaciers, at the terminus for one marine terminating glacier and halfway between the ice divide and terminus for another. Peak velocity also occurred at lower elevations (~100 m) for marine terminating glaciers than for land terminating glaciers (~400 m). While the smallest seasonal changes in flow speed were observed for the two smallest (lake terminating) glaciers, our results reveal that glaciers draining the FIIC exhibit a wide range of seasonality. We suggest that detailed study of individual outlet glaciers is required to improve our understanding of the processes governing the ice dynamics of similar ice masses.

[29] **Acknowledgments.** This work formed part of S. Palmer's Ph.D., which was funded by the UK Natural Environment Research Council via the Centre for Polar Observation and Modeling. The raw SAR data used in this study were obtained through the ESA VECTRA program. ICESat GLA06 and Greenland DEM data were obtained from the U.S. National Snow and Ice Data Center. Station Nord automatic weather station temperature data were obtained from the Tutiempo Network, www.tutiempo.net. Landsat data were obtained from the Global Land Cover Facility, www.landcover.org. We thank the three anonymous reviewers for their comments, which greatly improved the manuscript.

References

Atwood, D. K., R. M. Gurtiz, R. R. Muskett, C. S. Lingle, J. M. Sauber, and J. T. Freymuller (2007), DEM control in Arctic Alaska with ICESat laser altimetry, *IEEE Trans. Geosci. Remote Sens.*, *45*(11), 3710–3720, doi:10.1109/TGRS.2007.904335.

Bartholomew, I., P. Nienow, D. Mair, A. Hubbard, M. A. King, and A. Sole (2010), Seasonal evolution of subglacial drainage and acceleration in a Greenland outlet glacier, *Nat. Geosci.*, *3*(408), doi:10.1038/NGEO863.

Bingham, R. G., P. W. Nienow, and M. J. Sharp (2003), Intra-annual and intra-seasonal flow dynamics of a High Arctic polythermal valley glacier, *Ann. Glaciol.*, *37*, 181–188, doi:10.3189/172756403781815762.

Boon, S., and M. Sharp (2003), The role of hydrologically driven ice fracture in drainage system evolution on an Arctic glacier, *Geophys. Res. Lett.*, *30*(18), 1916, doi:10.1029/2003GL018034.

Brenner, A. C., et al. (2003), Derivation of range and range distributions from laser pulse waveform analysis for surface elevations, roughness, slope, and vegetations heights, Algorithm Theoretical Basis Document, v.4.1, Cent. for Space Res., Univ. of Texas at Austin, Austin. (Available at http://www.csr.utexas.edu/glas/atbd.html.)

Dall, J., S. N. Madsen, K. Keller, and R. Forsberg (2001), Topography and penetration of the Greenland Ice Sheet measured with airborne SAR interferometry, *Geophys. Res. Lett.*, *28*, 1703–1706, doi:10.1029/2000GL011787.

Das, S. B., I. Joughin, M. D. Behn, I. M. Howat, M. A. King, D. Lizarralde, and M. P. Bhatia (2008), Fracture propagation to the base of the Greenland Ice Sheet during supraglacial lake drainage, *Science*, *320*, 778–781, doi:10.1126/science.1153360.

DiMarzio, J. P., A. C. Brenner, and H. J. Zwally (2004), Comparison of Envisat and ERS radar altimetry for ice sheet elevation change studies, paper presented at Envisat and ERS Symposium, Eur. Space Agency, Salzburg, Austria, 6–10 Sept.

DiMarzio, J., A. Brenner, R. Schutz, C. A. Shuman, and H. J. Zwally (2007), GLAS/ICESat 1 km Laser Altimetry Digital Elevation Model of Greenland, http://nsidc.org/data/nsidc-0305.html, Natl. Snow and Ice Data Cent., Boulder, Colo.

Gens, R., and J. L. van Genderen (1996), Analysis of the geometric parameters of SAR interferometry for spaceborne systems, *Int. Arch. Photogramm. Remote Sens.*, *31*, 107–110.

Goldstein, R. M., H. Engelhardt, B. Kamb, and R. M. Frolich (1993), Satellite radar interferometry for monitoring ice sheet motion: Application to an Antarctic ice stream, *Science*, *262*, 1525–1530, doi:10.1126/science.262.5139.1525.

Hall, D. K., J. E. Box, K. A. Casey, S. J. Hook, C. A. Shuman, and K. Steffen (2008), Comparison of satellite-derived and in-situ observations of ice and snow surface temperatures over Greenland, *Remote Sens. Environ.*, *112*, 3739–3749, doi:10.1016/j.rse.2008.05.007.

Helk, J. V., and M. Dunbar (1953), Ice islands: Evidence from North Greenland, *Arctic*, *6*(4), 263–271.

Higgins, A. K. (1991), North Greenland glacier velocities and calf ice production, *Polarforschung*, *60*(1), 1–23.

Hoen, E. W., and H. A. Zebker (2000), Penetration depths inferred from interferometric volume decorrelation observed over the Greenland Ice Sheet, *IEEE Trans. Geosci. Remote Sens.*, *38*(6), 2571–2583, doi:10.1109/36.885204.

Iken, A. (1974), Velocity fluctuations of an Arctic valley glacier: A study of the White Glacier, Axel Heiberg Island, Canadian Arctic Archipelago, Ph.D. dissertation, McGill Univ., Montreal, Que., Canada.

Iken, A., and M. Truffer (1997), The relationship between subglacial water pressure and velocity of Findelengletscher, Switzerland, during its advance and retreat, *J. Glaciol.*, *43*(144), 328–338.

Joughin, I., and L. Padman (2003), Melting and freezing beneath Filchner-Ronne Ice Shelf, Antarctica, *Geophys. Res. Lett.*, *30*(9), 1477, doi:10.1029/2003GL016941.

Joughin, I. R., D. P. Winebrenner, and M. A. Fahnestock (1995), Observations of ice-sheet motion in Greenland using satellite radar interferometry, *Geophys. Res. Lett.*, *22*, 571–574, doi:10.1029/95GL00264.

Joughin, I., D. Winebrenner, M. Fahnestock, R. Kwok, and W. Krabill (1996), Measurement of ice-sheet topography using satellite-radar interferometry, *J. Glaciol.*, *42*(140), 10–22.

Joughin, I. R., R. Kwok, and M. A. Fahnestock (1998), Interferometric estimation of three dimensional ice-flow using ascending and descending passes, *IEEE Trans. Geosci. Remote Sens.*, *36*(1), 25–37, doi:10.1109/36.655315.

Kelly, M. A., and T. V. Lowell (2009), Fluctuations of local glaciers in Greenland during latest Pleistocene and Holocene time, *Quat. Sci. Rev.*, *28*, 2088–2106, doi:10.1016/j.quascirev.2008.12.008.

Koch, L. (1935), A day in North Greenland, *Geogr. Ann., Ser. A, Phys. Geogr.*, *17*, 609–620.

Krabill, W., W. Abdalati, E. Frederick, S. Manizade, C. Martin, J. Sonntag, R. Swift, R. Thomas, W. Wright, and J. Yungel (2000), Greenland Ice Sheet: High-elevation balance and peripheral thinning, *Science*, *289*, 428–430, doi:10.1126/science.289.5478.428.

Kwok, R., and M. A. Fahnestock (1996), Ice sheet motion and topography from radar interferometry, *IEEE Trans. Geosci. Remote Sens.*, *34*(1), 189–200, doi:10.1109/36.481903.

Maidment, D. R. (Ed.) (2002), *ArcHydro: GIS for Water Resources*, ESRI Press, Redlands, Calif.

Massonnet, D., and K. L. Feigl (1998), Radar interferometry and its application to changes in the Earth's surface, *Rev. Geophys.*, *36*, 441–500, doi:10.1029/97RG03139.

Mikkelsen, E. (1913), Expedition to north-east Greenland, 1909–1912, *Geogr. J.*, *41*(4), 313–322.

Mohr, J. J. (1997), Repeat track SAR interferometry: An investigation of its utility for studies of glacier dynamics, Ph.D. thesis, Tech. Univ. of Denmark, Copenhagen.

Paterson, W. S. B. (1994), *The Physics of Glaciers*, 3rd ed., 480 pp., Pergamon, Oxford, U. K.

Pritchard, H. D., R. J. Arthern, D. G. Vaughan, and L. A. Edwards (2009), Extensive dynamic thinning on the margins of the Greenland and Antarctic ice sheets, *Nature*, *461*, 971–975, doi:10.1038/nature08471.

Rignot, E. (1998), Fast recession of a West Antarctic glacier, *Science*, *281*, 549–551, doi:10.1126/science.281.5376.549.

Rosen, P. A., C. W. Werner, and A. Hiramatsu (1994), Two-dimensional phase unwrapping of SAR interferograms by charge connection through neutral trees, in *IGARSS '94: International Geoscience and Remote Sensing Symposium*, Inst. of Electri. and Electron. Eng., Piscataway, N. J.

Scharroo, R., and P. N. Visser (1998), Precise orbit determination and gravity field improvement for the ERS satellites, *J. Geophys. Res.*, *103*, 8113–8127, doi:10.1029/97JC03179.

Schutz, B. E., H. J. Zwally, C. A. Shuman, D. Hancock, and J. P. DiMarzio (2005), Overview of the ICESat Mission, *Geophys. Res. Lett.*, *32*, L21S01, doi:10.1029/2005GL024009.

Shepherd, A., D. J. Wingham, J. A. D. Mansley, and H. F. J. Corr (2001), Inland thinning of Pine Island Glacier, West Antarctica, *Science*, *291*, 862–864, doi:10.1126/science.291.5505.862.

Shepherd, A., A. Hubbard, P. Nienow, M. King, M. McMillan, and I. Joughin (2009), Greenland ice sheet motion coupled with daily melting in late summer, *Geophys. Res. Lett.*, *36*, L01501, doi:10.1029/2008GL035758.

Steffen, K., and J. Box (2001), Surface climatology of the Greenland ice sheet: Greenland climate network 1995–1999, *J. Geophys. Res.*, *106*, 33,951–33,964, doi:10.1029/2001JD900161.

Werner, C., U. Wegmüller, T. Strozzi, and A. Wiesmann (2000), Gamma SAR and interferometric processing of software, paper presented at Envisat and ERS Symposium, Eur. Space Agency, Gothenburg, Sweden, 16–20 Oct.

Zwally, H. J., W. Abdalati, T. Herring, K. Larson, J. Saba, and K. Steffen (2002a), Surface melt-induced acceleration of Greenland ice-sheet flow, *Science*, *297*, 218–222, doi:10.1126/science.1072708.

Zwally, H. J., et al. (2002b), ICESat's laser measurements of polar ice, atmosphere, ocean and land, *J. Geodyn.*, *34*, 405–445, doi:10.1016/S0264-3707(02)00042-X.

Zwally, H. J., R. Schutz, C. Bentley, J. Bufton, T. Herring, J. Minster, J. Spinhirne, and R. Thomas (2003), GLAS/ICESat L1B Global Elevation Data V018, http://nsidc.org/data/gla06.html, Natl. Snow and Ice Data Cent., Boulder, Colo (updated 2009).

P. Nienow and E. Rinne, School of GeoSciences, University of Edinburgh, Drummond Street, Edinburgh EH9 8XP, UK.

S. J. Palmer, A. Shepherd, and A. Sundal, School of Earth and Environment, University of Leeds, Maths/Earth and Environment Bldg., Leeds LS2 9JT, UK. (palmersteven@hotmail.com)